Colloids and Surfaces B: Biointerfaces 230 (2023) 113490

Contents lists available at ScienceDirect

Colloids and Surfaces B: Biointerfaces

journal homepage: www.elsevier.com/locate/colsurfb

The role of hydrophobic interactions in the molten globule state of globular protein modulated by surfactants

Yang Sun [a,*,1], Pedro L. Oseliero Filho [b,1], Yang Song [a], Zhichun Wang [a], Hang Ji [a], Cristiano L. P. Oliveira [b,*]

[a] College of Vocational and Technical Education, Yunnan Normal University, Kunming, Yunnan, China
[b] Instituto de Física, Universidade de São Paulo, São Paulo, Brazil

ARTICLE INFO

Keywords:
Hydrophobic interactions
Molten globule state
Bovine α-lactalbumin
Alkyl trimethylammonium bromides
SAXS

ABSTRACT

In order to highlight the role of hydrophobic interactions in the molten globule (MG) state of globular protein modulated by surfactants, the interactions of bovine α-lactalbumin (α-LA) with alkyl trimethylammonium bromides (C_nTAB, $n = 10$, 12, 14, and 16) have been studied by experimental and theoretical techniques. Isothermal titration calorimetry (ITC) showed that the enthalpy changes (ΔH) and area of the enthalpogram increased with increasing the chain length of C_nTAB. The result of fluorescence, circular dichroism (CD) and ^{1}H nuclear magnetic resonance (NMR) spectrum suggested that C10TAB and C12TAB unfolded α-LA partially, C14TAB reconstructed protein with a native-like secondary structure content, and C16TAB induced an MG state α-LA. The SAXS results confirmed that the tertiary structure of α-LA was disrupted by C16TAB forming an MG state complex with a micelle-like structure even at the surfactants concentrations below CMC. As indicated by MD results, the β-domain and unstructured region(s) were involved in the MG state α-LA modulated by C_nTAB. This work not only provides molecular insights into the role of hydrophobic interactions in the MG state of a globular protein but also helps understand the mechanism of preparing α-LA based biomacromolecule modulated by hydrophobic interactions.

1. Introduction

Protein–surfactant interactions are of great significance for basic research in life science, biomedicine, drug development, etc. They also have extensive applications in the food industry, pharmaceutical industry, and, not the least, fabric and homecare detergent industry [1]. Sodium dodecyl sulfate-polyacrylamide gel electrophoresis (SDS-PAGE) owes the most prevalent as an analytical tool in protein science to the capacity of SDS to denature proteins [2]. Previous studies [3–7] concluded that protein–surfactant interactions can be multi-step. Although details differ from protein to protein, surfactant to surfactant, the first stage involves the association of a few individual surfactant monomers with the protein, and the subsequent step generally leads to the modification or reconstruction of the protein's structure (depending on the nature of surfactant). In this stage, the change in the structure of the protein develops over time, in which many intermediate states of the protein-surfactant complex have been detected and confirmed after a few milliseconds to seconds by experimental and theoretical simulation techniques [8–10]. When the surfactant is present at a sufficiently high concentration to achieve the saturation binding step.

Motivated by the widespread applications of surfactants, many investigations have been devoted to the understanding protein-surfactant interactions, both in the bulk and at interfaces [11]. Saha et al. [12] reported that the unfolding of bovine serum albumin (BSA) increased with increasing the chain length of the *n*-alkyl trimethylammonium bromide surfactants. Andersen and Otzen [13] revealed that ionic surfactants with shorter alkyl chains lead to dramatically slower denaturation protein kinetics with the expected reduction in binding affinity and unfolding rates. Moreover, Højgaard et al. [2] studied that a protein completely lacking charged side chains was unfolded by SDS in a manner similar to charged proteins, suggesting that formal protein charges were not required for SDS-induced protein unfolding or binding. Despite extensive investigations focusing on such interactions, there are

* Corresponding authors.
E-mail addresses: sunyang@hbuas.edu.cn (Y. Sun), crislpo@if.usp.br (C.L.P. Oliveira).
[1] These authors are equal to this work.

https://doi.org/10.1016/j.colsurfb.2023.113490
Received 26 April 2023; Received in revised form 25 June 2023; Accepted 31 July 2023
Available online 3 August 2023

still outstanding issues, mainly because such interactions are molecule-specific and vary significantly with the size and nature of the surfactants as well as the relative contribution of hydrophobic interactions to the intermediate states under research [11].

One of the best-studied intermediate states is that formed by α-lactalbumin (α-LA). As a model globular protein, α-LA contains 123 amino acid residues and has a molecular mass of 14.2 kD. The structure of α-LA is divided into two domains, one is mainly helical (the α-domain) and the other has a significant content of β-sheet (the β-domain). In the condition of pH-range 4.2–3 and above pH 9.5, moderate guanidinium chloride concentrations, or elevated temperatures (apo-form), α-LA forms a compact globular structure (the A-state) that lacks the specific side chain packing that is characteristic of native conformation, which is commonly termed molten globule (MG) state by substantial secondary structure arranged in an overall native-like fold, a compact shape, formation of hydrophobic core exposed to solvent, and the absence of tertiary structure [14,15]. The MG state is an equilibrium unfolding intermediate under mildly denaturing conditions of many globular proteins such as α-LA, cytochrome *c* and apomyoglobin [16].

In order to highlight the role of hydrophobic interactions in the intermediate states of globular protein modulated by surfactants, we have investigated the unfolded and MG state of α-LA induced by ammonium bromide surfactant with different chain length (C_nTAB, $n = 10,12,14,16$) using isothermal titration calorimetry (ITC), fluorescence and circular dichroism (CD) spectra, small-angle x-ray scattering (SAXS) as well as molecular dynamics (MD) simulation. This work not only describes the overall binding of C_nTAB with α-LA in the secondary structure and conformation but also provides more insights into the role of hydrophobic interactions in the MG state of globular protein modulated by surfactants.

2. Materials and methods

2.1. Materials

Bovine α-lactalbumin (α-LA, ≥95%), decyl-trimethylammonium bromide (C10TAB, ≥98%), dodecyl-trimethylammonium bromide (C12TAB, ≥98%), myristyl-trimethylammonium bromide (C14TAB, ≥98%) and trimethyl-stearylammonium bromide (C16TAB, ≥98%) were purchased from Sigma-Aldrich (St. Louis, USA) and used without further purification. All samples were prepared with 10 mM pH 7.0 PBS buffer. Ultra-high-purity water was prepared using a Millipore SAS-67120 (Molsheim, Cedex, France).

2.2. Isothermal titration calorimetry (ITC)

The ITC measurements were performed with a MicroCal iTC_{200} (GE Healthcare Life Sciences). Briefly, 200 μL buffer or α-LA solution with concentration of 30, 60, 90, 120 or 150 μM was injected into the sample cell and then was titrated by C_nTAB solution in a 40 μL syringe. The concentration of C_nTAB was approximately ten times higher than its critical micellar concentration (CMC) (CMC of C_nTAB (n = 10, 12, 14 and 16) is 60, 8, 2 and 0.1 mM respectively [7]). For each titration step, a volume of 1 μL of C_nTAB solution was injected into the cell. The obtained heat flux signals (the *fluxogram*) were integrated by the Origin™ software supplied by MicroCal™ to obtain the corresponding ΔH value of the enthalpogram.

2.3. Fluorescence spectrum

Steady-state fluorescence measurements of the α-LA solution (30 μM) containing different concentrations of C_nTAB injected into a 10 mm quartz cuvette (Hellma, Germany) were carried out using Cary Eclipse fluorescence spectrophotometer (Varian Ltd.) with an excitation wavelength of 280 nm and an emission range between 285 and 450 nm. Both excitation and emission slits widths were set at 5 nm with a scanning speed 200 nm/min for an average of three accumulations. The background correction was conducted using pH 7.0 PBS buffer. All measurements were performed at 25 °C.

2.4. Far- and near-UV circular dichroism (CD) spectra

Far-UV and near-UV circular dichroism (CD) spectra were recorded on a JASCO J-810 spectropolarimeter (Jasco, Japan). Wavelength scans were recorded in the range of 195–260 nm (bandwidth 0.5 nm and path 0.1 cm) for far-UV CD and 250–320 nm (bandwidth 1.0 nm and path 0.5 cm) for near-UV CD. The scanning speed was 10 nm/min with 4 s of response for three accumulations. Background contributions from the buffer were subtracted. The results were presented as the mean residue molar ellipticity [θ] (deg cm^2 $dmol^{-1}$) *versus* wavelength (nm). The secondary content of protein was analyzed using deconvolution software CDNN2.1 (Circular Dichroism analysis using Neural Networks) (http://gerald-boehm.de/download/cdnn) [17]. The background correction was conducted using pH 7.0 PBS buffer. All measurements were performed at 25 °C. According to the X-ray study of bovine α-LA in a hexamer state, α-LA contains three major helices per monomer consisting of 38 residues [18]. The residue number of the major α-helix segments accounts for 31–32% of the 123 residues. The curve-fitting of the CD spectrum of bovine α-LA has been reported to give the helical content of 34% at 25 °C [19–21]. The concentration of α-LA used was 0.015 and 0.03 mM for far-UV and near-UV CD, and the C_nTAB to protein ratio was derived from the stoichiometry of ITC. The original helical content was used throughout the present paper.

2.5. Nuclear magnetic resonance (NMR) measurements

NMR measurements were performed on a 600 MHz Bruker spectrometer equipped with a field gradient probe (located at Tsinghua University). NMR tubes (5-mm) were used with accounting D_2O of 30%. A total of eight scans were collected with a recycling delay of 1 s. In each run, eight dummy scans were applied to the sample before the actual experiment was carried out. For protein self-diffusion measurements, the spectral width was 20 ppm and 16 scans were collected with a recycling delay of 2 s. All 1D ^{1}H NMR data were Fourier transformed with 0.3- to 1.0-Hz exponential line broadening. All the measurements were performed at 25 °C.

2.6. Small angle X-ray scattering (SAXS)

All SAXS measurements were performed on the BL19U2 beamline at NFPS (Shanghai, China), equipped with a robotic sample changer and a Pilatus 1 M detector (DECTRIS, Ltd.) with an exposure time of 1 s [22]. The wavelength of the incoming monochromatic X-ray beam is $\lambda = 1.54$ Å with a q-region from 0.009 to 0.437 $Å^{-1}$. The resulting data is displayed as a function of the modulus of the scattering vector q, where q is defined as $q = 4\pi\sin(\theta)/\lambda$, where 2θ is the scattering angle. All measurements were performed at 25 °C. Buffer subtraction from samples, data reduction and normalization with transmitted beam intensity were performed using BioXTAS RAW software (Version 1.2.1) [23]. SAXS data analysis was carried out by the ATSAS software program suite (Version 3.0.0) [24]. The CRYSOL was employed to evaluate the experimental solution SAXS data from α-LA with theoretical scattering data from atomic structure, and the goodness of fitting is determined by the discrepancy value (χ^2) between theoretical and experimental data as well as visual inspection [25]. The *ab initio* models were reconstructed by the DAMMIN with a q-range of 0.009–0.437 $Å^{-1}$ [26]. Thirty independent runs were performed and the resulting models were averaged by DAMAVER [27] and filtered by DAMFILT to generate the final model. The alignment of the atomic structure with the *ab initio* model was superimposed using SUPCOMB program [28] based on the normalized spatial discrepancy (NSD) criteria.

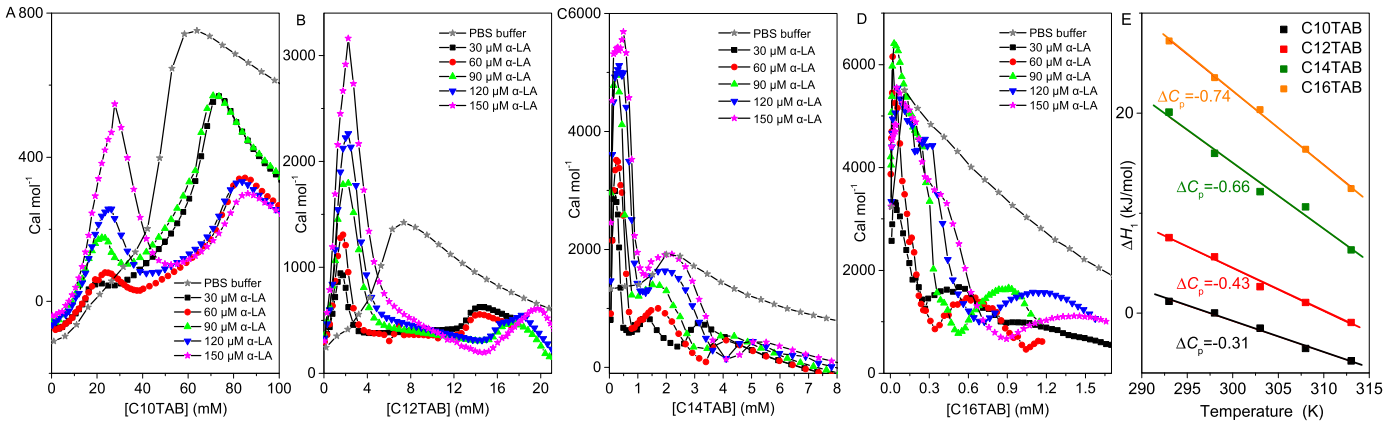

Fig. 1. ITC curve of titrated C10TAB (A), C12TAB (B), C14TAB (C) and C16TAB (D) into PBS buffer and various concentrations of α-LA. (E): Plot of variation of ΔH_1 (in kJ mol^{-1}) as a function of temperature for the binding of C_nTAB with α-LA, ΔC_p values in kJ mol^{-1} K^{-1}.

2.7. Molecular dynamic (MD) simulation

MD simulations and subsequent analyses were carried out with the GROMACS 2018.2 package. The AMBER99SB-ILDN force field was used for the α-LA alone and the gaff2 force field was used for the α-LA containing 40, 20, 10 or 5 C10TAB, C12TAB, C14TAB or C16TAB molecules according to the ITC inflection points. A cubic box with a minimum spacing of 1 nm for all edge-to-protein distances was used as the simulation box to solvate α-LA with transferable intermolecular potential with three points (TIP3P) for water molecules, and a specified number of surfactants were added to the box randomly using the insert-molecules command in GROMACS. The complex was then neutralized by adding counterions (Na^+/Cl^-) with an ionic strength of 10 mM [29]. The systems were initially minimized energetically through 10,000 steps with the steepest descent methods [30]. Then the system was heated to 300 K in the canonical ensemble (NVT) during 100 ps MD simulation and equilibrated for another 100 ps in the isothermal-isobaric (NPT) ensemble. The production run was performed for 300 ns for protein and each complex. During the simulation, the LINCS algorithm was used to constrain the bond length [31]. MD simulations were run with a 2 fs time step. Isothermal and isobaric coupling constants were kept at 0.1 ps and 2 ps, respectively, bringing the system to a stable environment of 300 K temperature and 1 bar pressure. A 10 Å cut-off was enforced to restrict short-range interactions, while van der Waals interactions were restricted to 14 Å. The trajectory was saved every 60 ps. The stability of the dynamic system was evaluated by the values of the radius of gyration (R_g), root mean square deviation (RMSD) and root mean square fluctuation (RMSF) derived from GROMACS. The secondary structure of α-LA was analyzed by the DSSP program [32]. The automated force field topology builder obtained the original coordinates of C_nTAB molecules [33,34].

3. Results and discussion

3.1. Thermodynamic of binding of C_nTAB to α-LA

The isothermal titration calorimetry (ITC) enthalpogram profiles of C_nTAB titrated into series concentrations of α-LA (30–150 μM) were determined. The enthalpogram behavior of C_nTAB titrated into PBS buffer has been investigated previously and the critical micellar concentration (CMC) of C_nTAB ($n = 10$, 12, 14 and 16) is found to be 50 mM, 6 mM, 2 mM and 0.25 mM, respectively [7]. As seen from Fig. 1, the shape of the α-LA ITC curve varies from C10TAB to C16TAB and the enthalpy change (ΔH) profile obtained by the endothermic peak as well as exothermic peak area increases with increasing concentrations of protein, demonstrating that the larger protein amounts need more C_nTAB molecules to meet unfolding and structural reconstruction, and thus led to an increased ΔH [5].

The ITC curves show the first peak between 10 and 40 mM C10TAB, 1–6 mM C12TAB, 0–1 mM C14TAB and 0–0.3 mM C16TAB, which indicates that α-LA unfolding event induced by C_nTAB is endothermic ($\Delta H > 0$) as the contribution from breaking hydrogen bonds out-weighs the contribution of the exothermic events such as the neutralization of cationic C_nTAB with negative charged α-LA (isoelectric point of ~4.3) and disruption breaking of hydrophobic interactions [35]. Subsequently, the second endothermic behavior is observed between 60 and 100 mM C10TAB and 12–20 mM C12TAB, suggesting binding of saturation and the free C10TAB or C12TAB micelles formation. The ITC curves of C10TAB and C12TAB titrated into α-LA are similar to the those of C_nTAB titrated into caseinate, where the caseinate particles are dissociated into casein clusters by C_nTAB [7].

However, besides the endothermic peak in the ITC curve of α-LA titrated by C_nTAB with a longer alkyl chain ($n = 14$ and 16), an exothermic minimum at 2.5–4 mM C14TAB and 0.9–1.9 mM C16TAB is observed, implying that the unfolded protein undergoes structural reconstruction before free micelles formation. It is hard to calculate the exact minimum of C16TAB titrated into higher α-LA concentrations due to the difficulty of increasing C16TAB concentration in a syringe. Interestingly, the C14TAB and C16TAB titration behavior into α-LA shows the similarity with the ITC curve of SDS into α-LA, in which the structural rearrangement, cooperative unfolding and refolding of α-LA with increasing α-helical content upon bound by SDS has been reported [5].

Meanwhile, ΔH obtained from the first endothermic peak of α-LA bound by C_nTAB ($n = 10$, 12, 14 and 16) is calculated as 0.83, 2.85, 13.48 and 15.73 kJ mol^{-1}, demonstrating that the more considerable enthalpy change induced by the longer alkyl chain of C_nTAB. Moreover, the association of α-LA with C_nTAB is spontaneous and the Gibbs free energy (ΔG) is negative; thus, the binding characterizes as a favorable entropic contribution ($\Delta S > 0$), suggesting that the hydrophobic interaction plays a dominant role in the binding of α-LA with C_nTAB. This result indicates that the binding of α-LA with C_nTAB is a predominant enthalpic contribution to the overall free energy change (ΔG_1) of the process [36]. On the other hand, the ΔH_2 of surfactant micellization decreases at higher α-LA concentrations, which means that the ΔH_2 generated by free C_nTAB micelles formation is reduced by association with α-LA and the mixed micellization of C_nTAB-α-LA is preferable [37].

Then, the variation of ΔH_1 of the C_nTAB-α-LA binding with temperature has been processed to investigate the constant pressure heat capacity change (ΔC_p) according to the standard thermodynamic relationship [36]:

$$\Delta C_p = d(\Delta H)/dT$$

The variations of ΔH_1 of C_nTAB bound by α-LA as a function of

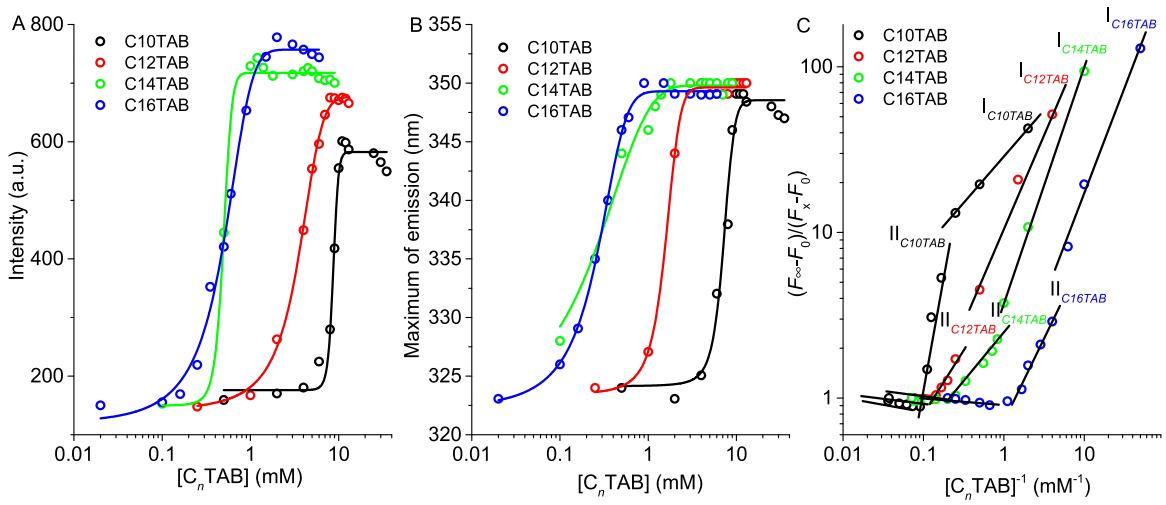

Fig. 2. Effect of different concentrations of C$_n$TAB (n = 10, 12, 14 and 16) on the fluorescence intensity (A) and maximum emission (B) of α-LA (0.03 mM). C: Corresponding modified Benesi-Hildebrand curves of α-LA bound by C$_n$TAB.

temperature are shown in Fig. 1E. The sign and magnitude of ΔC_p can provide a crucial reference for molecular-level explanations of binding force properties under interactions. The value of ΔC_p for α-LA bound by C$_n$TAB (n = 10, 12, 14 and 16) is calculated by the slope of the plot as − 0.31, 0.43, − 0.66 and − 0.74 kJ·mol^{-1}K^{-1}, which reflects a typical thermodynamic signature corresponding to the release of water of hydrophobic hydration and/or counterions from the hydrophobic surfaces on α-LA upon C$_n$TAB bound [36]. The classical hydrophobic interactions, in which nonpolar surfaces are shielded from bulk water, are characterized by a favorable entropic binding signature together with a negative ΔC_p [38]. Nevertheless, while the ΔS is significantly temperature dependent, the heat capacity change is not, and ΔS is positive for the solvation of polar solutes. At the same time ΔC_p is negative, demonstrating that the ΔC_p may be a more prominent feature of the hydrophobic interactions [39]. The release of ordered water from the transfer of nonpolar surfaces into the hydrophobic core of the protein accompanies a decrease in the heat capacity bound by C$_n$TAB and thus leads to a negative ΔC_p [40]. C$_n$TAB with a longer alkyl chain contributes more hydrophobic interactions during the binding process, which also reasonably explains the favorable entropic contribution to the interaction with the increasing chain length of C$_n$TAB ($T\Delta S_1 > 0$). The result demonstrates that the association of α-LA with C$_n$TAB comprises several hydration contributions and hydrophobic interaction force dominates the binding process, and the shielding of hydrophobic (or nonpolar) molecular surfaces from the aqueous phase due to the association plays a significant role in the negative heat capacity change.

3.2. Structural change of α-LA upon bound by C$_n$TAB

3.2.1. Fluorescence analysis

The fluorescence properties of bovine α-LA are mainly due to four tryptophan (Trp) residues, Trp-26, Trp-60, Trp-104, and Trp-118. Trp-26 is in the β-sheet domain and Trp-60 sandwiches between the α-helical and the β-sheet domain may act as a reporter for the structure reconstruction of the β-sheet domain. Trp-104 is located in the hydrophobic box region surrounded by the helices B-D in the hydrophobic cluster II [41]. Trp-118 is located between the B- and C-terminal 310-helices in the hydrophobic cluster I [42], which has been shown previously to be essential for the folding and stability of the MG state α-LA [43,44].

As displayed in Fig. S2 and Fig. 2A and 2B, the fluorescence feature of α-LA undergoes a sigmoidal transition with a three-stage change upon C$_n$TAB bound, in which the intensity increases slightly along with a gentle red-shift in the maximum emission from 325 nm to 328 nm in the initial addition of C$_n$TAB. Subsequently, with the increase of C$_n$TAB concentration, a significant improvement of intensity accompanying a remarkable red-shift of the emission from 328 nm to 350 nm was observed. This result indicates that Trp residues were exposed to the solvent and the environment of the Trp residues was more hydrophilic when binding with C$_n$TAB. The reconstruction of α-LA by the further association of C$_n$TAB leads Trp residues to remain in the hydrophilic environment with more solvent exposure. It is comparable that the solvent- or heat-mediated α-LA denaturation leads to a significant increase in fluorescence intensity accompanied by a red shift in emission [45]. Additionally, the binding with C$_n$TAB promoted the contact and energy transfer from the lone pair electrons at the indole ring in Trp residues to the trimethylammonium bromide group of C$_n$TAB, which may also lead to the reduction in the fluorescence intensity of α-LA.

Table 1
Thermodynamic, binding and structural parameters of α-LA (30 μM) bound by C$_n$TAB.

Sample	Thermodynamic parameters				Secondary structural content (%)[c]			
	$\triangle H_1$[a] (kJ mol^{-1})	$\triangle H_2$[a] (kJ mol^{-1})	K_{a1}[b] (10^2 M^{-1})	K_{a2}[b] (10^2 M^{-1})	α-Helix	Antiparallel-Parallel	β-Turn	Randomly Coil
Native α-LA	-				31.4	19.2	20.2	30.2
C10TAB-α-LA	0.83	24.5	14.1	14.4	24.5	14.1	14.4	46.1
C12TAB-α-LA	2.85	30.6	17.4	16.9	30.6	17.4	16.9	35.1
C14TAB-α-LA	13.48	32.0	20.3	18.3	32.0	20.3	18.3	29.3
C16TAB-α-LA	15.73	33.2	23.6	15.1	33.2	23.6	15.1	28.1

[a] Calculated by ITC enthalpogram profile.
[b] Calculated by modified Benesi-Hildebrand curves
[c] Secondary structural content of native α-LA and α-LA bound by C$_n$TAB obtained from deconvolution of CD spectra in the far-UV region (190–260 nm) at 25 ℃ using the deconvolution software CDNN2.1

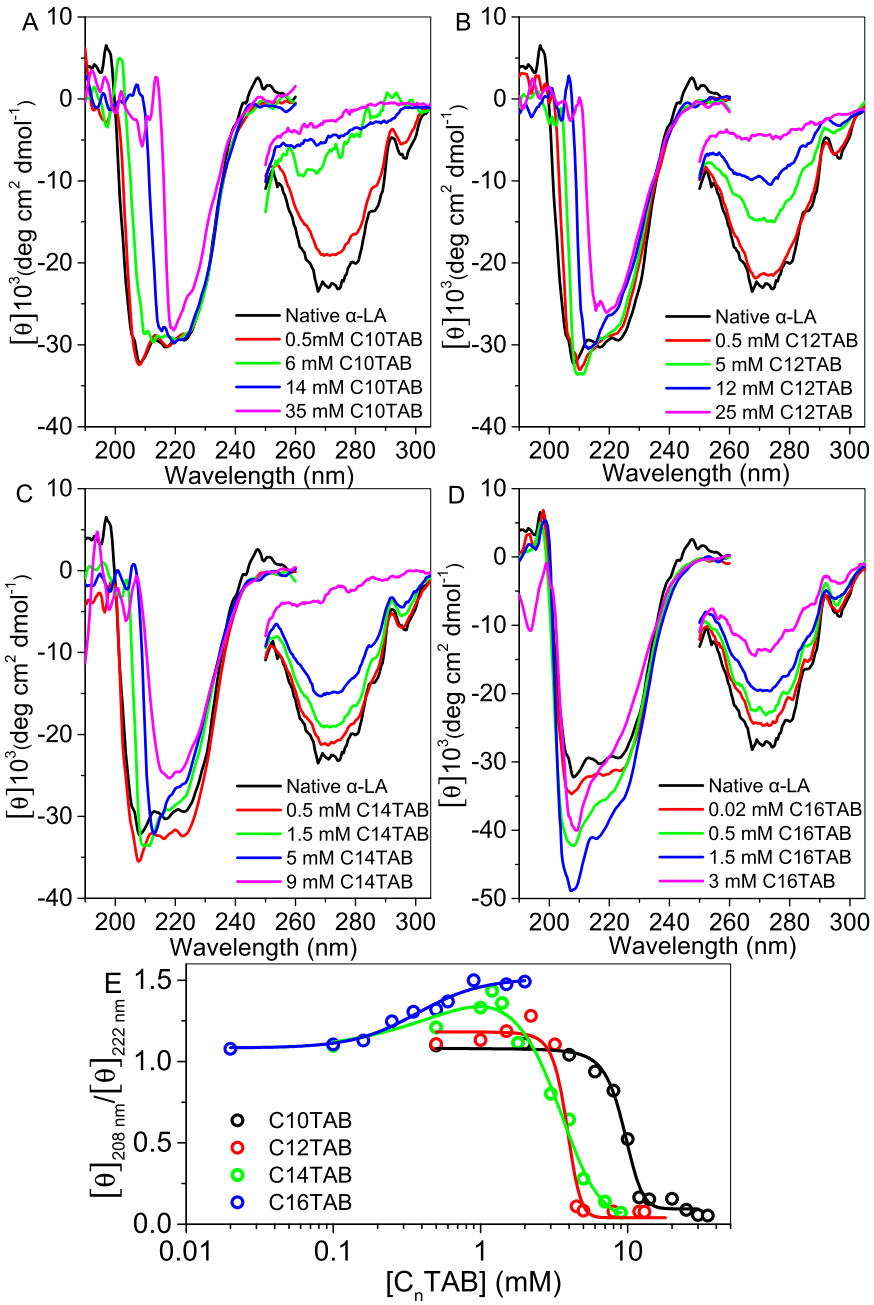

Fig. 3. A-D: Representative far-UV and near-UV CD spectra of α-LA in different concentrations of C_nTAB (n = 10, 12, 14 and 16), respectively. E: The plots of C_nTAB concentration with ellipticity at 208 nm and 222 nm of samples.

Little change in the intensity and emission on the higher C_nTAB concentrations was found meaning the saturation of binding process.

The binding and thermaodynamic parameters, such as binding constant and free energy, have been calculated by the modified Benesi-Hildebrand equation [46]: $\frac{F_\infty - F_x}{F_x - F_o} = 1 + \frac{1}{K_a[S]}$, where K_a represents the binding constant, F_o, F_x and F_∞ denotes the steady-state fluorescence intensities in the absence and presence of C_nTAB, respectively, and $[S]$ is the concentration of C_nTAB. The dependence of $(F_\infty - F_x)/(F_x - F_o)$ on the reciprocal value of the C_nTAB concentration $[C_nTAB]^{-1}$ was oberved to be linear with a slope equal to the value of $(K_a)^{-1}$. Fig. 2C displays the modified Benesi-Hildebrand plots, and the corresponding thermodynamic and binding parameters are presented in Table 1. As seen from Fig. 2C, upon binding with C_nTAB, α-LA undergoes a three-stage change in the spectral feature, where the first (I_{CnTAB}) and second linear part (II_{CnTAB}) of the plot corresponds to the lower and higher binding affinity of α-LA to C_nTAB. The binding constant K_{a1} of α-LA-C_nTAB (n = 10, 12, 14 and 16) is found to be 0.33, 0.57, 1.06 and 5.08 × 10^2 M^{-1} according to the slope of the linear fitting, and the value K_{a2} is calculated as 0.47, 5.57, 10.09 and 15.60 × 10^2 M^{-1}, respectively, suggesting that the C_nTAB with longer alkyl chain prefers binding with α-LA. This result is in line with the ITC results that the C_nTAB with longer alkyl chain contributed larger enthalpy change and the hydrophobic interaction dominated the α-LA bound by C_nTAB. Moreover, one can deduce that the association of α-LA with C_nTAB was accelerated sharply in the second state, and a longer alkyl chain of C_nTAB provided a higher affinity for C_nTAB with α-LA.

3.2.2. Circular dichroism (CD) analysis

The far-UV circular dichroism (CD) spectrum was used to monitor secondary structure changes of α-LA. Fig. 3 shows the CD characteristics

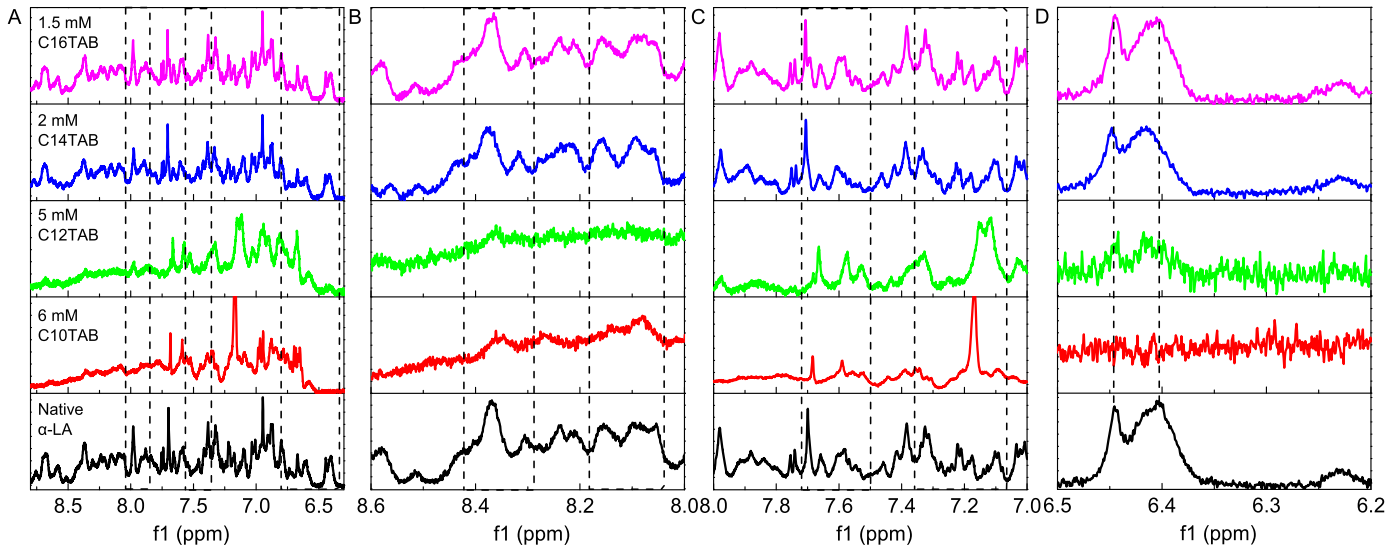

Fig. 4. Effect of different concentrations of C_nTAB ($n = 10$, 12, 14 and 16) on the ^1H NMR spectrum of α-LA.

of the secondary and tertiary structure of α-LA upon binding with C_nTAB, and plot of ellipticity at 208–222 nm ratio ($\theta_{208}/\theta_{222}$) as a function of C_nTAB concentrations. The contents of α-helix, β-turn and random coil have been calculated and summarized in Table 1. After the addition of C10TAB, C12TAB and C14TAB, the intensity of the negative band of far-UV CD presented a considerable decrease, but the valley around 218 nm, a typical feature of a β-sheet conformation was still observable. The near-UV CD was essentially featureless, and the intensity of the far-UV CD was greatly diminished, suggesting a loss of tertiary structure. As listed in Table 1, α-LA shows a decreased content of α-helical and β-turn conformation and an increased content of random coil conformation upon bound by C10TAB and C12TAB. Despite the considerable modification of C14TAB in the CD spectrum, α-LA was calculated as similar secondary content with the native state (Table 1). Moreover, the unfolding transition curves at an ellipticity ratio of 208 nm to that of 222 nm (Fig. 3E) are coincident with the fluorescence behavior, i.e., α-LA undergoes a three-stage C_nTAB-induced ($n = 10$, 12 and 14) unfolding transition (Fig. S1) where is different from the complete denaturation of α-LA.

By added with C16TAB (Fig. 3D), the far-UV CD of α-LA exhibited a significant enhancement in the ellipticity at ~208 and 222 nm with a sigmoidal transition of $\theta_{208}/\theta_{222}$ (Fig. 3E), and the intensity of near-UV CD was still visible. As listed in Table 1, the α-helical and parallel conformation increases and random coil content decreases. A protein's more helicity and partially rigid tertiary structure are a hallmark of the MG state α-LA upon C16TAB bound. A distinct difference appeared in the C_nTAB-induced structure of α-LA; the short-chain C_nTAB ($n = 10$ and 12) unfolded α-LA partially, and the medium-chain C14TAB reconstructed protein with a native-like secondary structure content. α-LA exhibited an MG state when bound by C16TAB. This result supports the study that the binding of C_nTAB led to the dissociation of the caseinate particles, and longer-chain C_nTAB showed a higher binding affinity forming a more stable C_nTAB-casein complex [7].

3.2.3. Nuclear magnetic resonance (NMR) analysis

The full ^1H NMR spectrum of native α-LA bound by C_nTAB was given in Fig. 4A, and three resonance regions (8.6–8.0 ppm; 8.0–7.0 ppm; 6.5–6.2 ppm) were enlarged in Fig. 4B-D. The ^1H NMR of C_nTAB showing the resonance characteristics at 3.0, 1.25, 0.75 ppm has been reported in previous work (Fig. S3) [7]. By bound with C10TAB and C12TAB, the ^1H NMR of α-LA has a broad and poorly resolved spectrum with an upfield-shift of resonance at 6.4 ppm and integrated as a single resonance at 7.3 ppm, which is comparable with the NMR spectrum of highly unfolded α-LA induced by 6 M GuHCl.

With the addition of C14TAB, the ^1H NMR of α-LA was considerably dispersed and well-resolved and differed markedly from the spectrum of the highly unfolded state, where the resonance of the aromatic ring of α-LA at 6.4 ppm showed an upfield-shift effect and the resonance at 8.6 ppm was diminished, as well as a single integrated resonance at 8.25 ppm was also observed. This indicates the presence of a disordered state intermediate between the fully unfolded and the native state [47]. Upon the addition of C16TAB, the ^1H NMR of α-LA showed an upfield-shift of resonance at 7.7 ppm and 6.4 ppm with an integrated resonance and 8.1 ppm. Meanwhile, as seen from Fig. S4, after added by C16TAB, the resonance of α-LA at 3.6 ppm, assigned as residue Trp-60, was reduced and resonance at 2.3 ppm, 3.2 ppm and 4.2 ppm, assigned as residues Asp-37-Ala-46, were more pronounced containing a series of well-resolved amide lines [48]. This result not only suggests a direct interaction of these residues with C16TAB and changes in their local environment upon bound by C16TAB, but the lack of persistent tertiary structure needed to give rise to resonances significantly perturbed from those found in the partially unfolded state [47].

The random coil region containing residues Gly-35–Ile-46 shows a helical propensity and forms a non-native helical structure in a high-temperature examination of the MG state α-LA [49]. This region is located in the β-domain and it is reported to be less stable than the α-domain, and its conversion to helices upon partial denaturation has been described or theorized [48]. The negatively charged residues, such as Glu-7, Glu-11, and Asp-97, could interact strongly with the oppositely charged C_nTAB. After the initial electrostatic binding, short-range van der Waals interactions between hydrophobic residues of α-LA and C_nTAB occured. Neutralization of negative charges on the protein surface by the C_nTAB may accelerate this process, which would first weaken the tertiary structure of α-LA, transiently exposing hydrophobic residues, then the binding with the longer C_nTAB alkyl chain provided a stronger bond which was more energetically favored. This resulted in the conversion of random-coil into the helical structure and thus the MG state of α-LA bound by C16TAB was observed. The helix A (residues 5–11) and helix C (residues 86–99) in α-LA contain the positively charged residues providing electrostatic repulsion and making a close approach unfavorable to the ammonium bromide group of C_nTAB, which may also display a degree of protection relative to the α-LA MG state [50]. Moreover, the association of C_nTAB with α-LA's random coil segment(s) may place Trp residue(s) at the C_nTAB cluster interface where the rest of the protein segments and the C_nTAB excluded the accessibility of the quencher, which was promoted by the longer alkyl

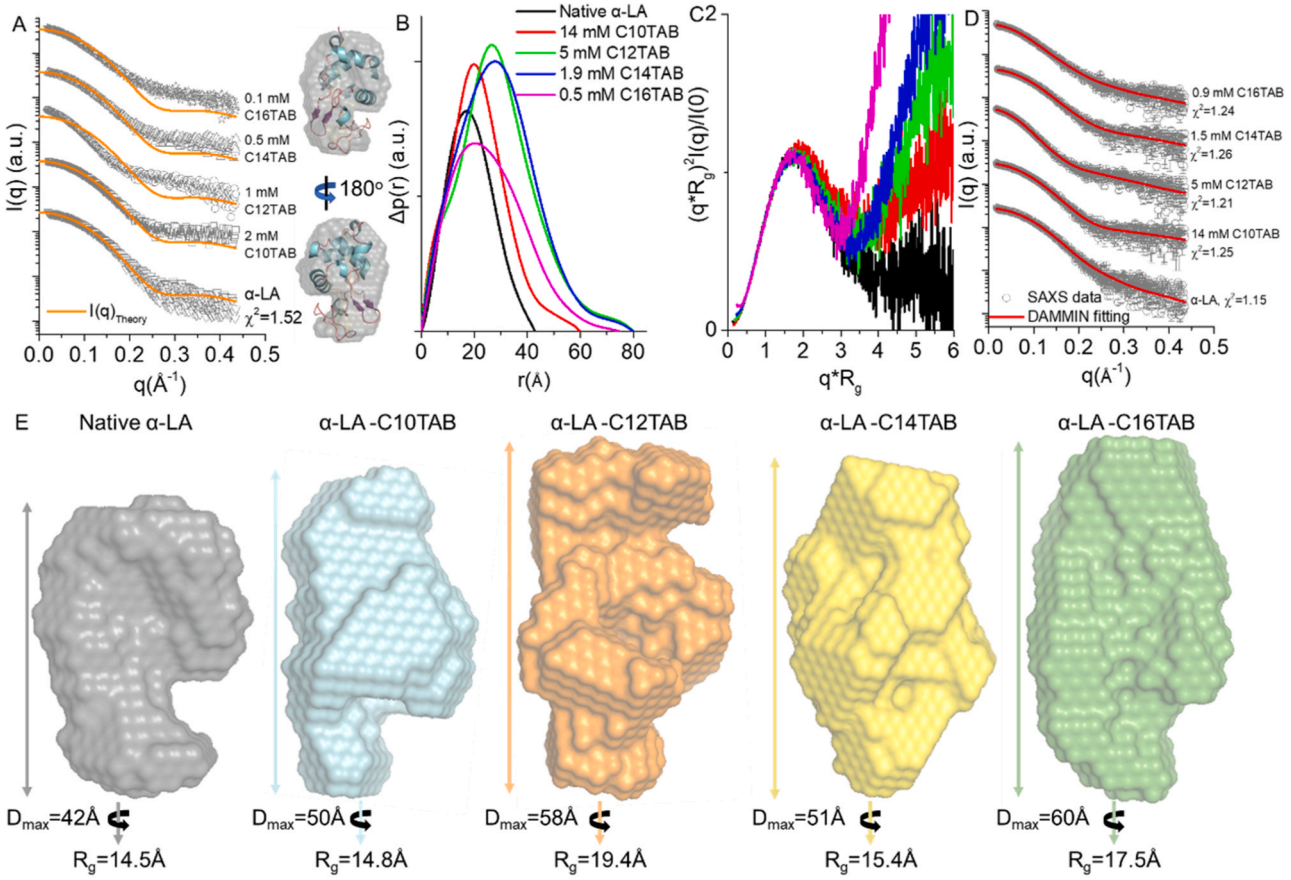

Fig. 5. A: *Left* pane: the fitting of experimental data of α-LA (open scatter) in the presence of different concentration of C_nTAB with the theoretical scattering intensity of crystal structure (PDB: 1A4V, solid line); *right* pane: *ab initio* shape envelope from DAMMIN overlays with α-LA crystal structure. B and C: corresponding pair-distance distribution, $p(r)$ curve and Kratky plot. D and E: Fitting of experimental data (open circles) with DAMMIN fitting (solid line) and corresponding envelope, goodness of fitting was evaluated by the χ^2-value.

chain C_nTAB. Trp-60 is in the random coil region and may approach the C_nTAB, and thus Trp-60 could be an appropriate candidate for being buried side-chain into being embedded its side-chain into the protein-C_nTAB cluster.

The results of fluorescence, CD and NMR spectrum confirm that the hydrophobic interactions play a critical role in the unfolding and refolding of protein modulated by surfactant and the surfactant association promotes the efficient of MG state because the protein has a loose tertiary structure that transiently exposes hydrophobic residues. This is in line with the study that the hydrophobic residues play a crucial role in stabilizing the protein MG state [51].

3.3. Analysis of solution structure

Small angle x-ray scattering (SAXS) has proven to be a powerful and fast technique for identifying the structure, folding state, and flexibility of biomacromolecules and complexes in solution [52]. The SAXS measurements have been performed and the scattering profiles are presented in Fig. 5 and Fig. S5. The overall structural parameters are summarized in Table S1. The SAXS profile of α-LA shows a typical feature of a globular protein, and the $p(r)$ curve is symmetric with a maximum interatomic distance (D_{max}) of 40 Å, the dimensionless Kratky plot $[(qR_g)^2I(q)/I(0)$ vs. $qR_g]$ presents a bell-like profile with a clear maximum and a regression to X-axis at higher q region, indicating a folded α-LA in solution. As seen from Fig. S5, with added by C_nTAB, the linearity observed in the Guinier plot (insert of Fig. S5B, $q_{max}{*}R_g < 1.3$) confirms the monodispersity of α-LA-C_nTAB complex and the good quality of data allows further analysis. A characteristic scattering "bump" in the q range of 0.1–0.3 $Å^{-1}$ with a dropped frequency around 20 Å in the $p(r)$ curve is observed, while the scattering profiles of α-LA-C_nTAB entirely differ from that of pure C_nTAB (Fig. S6). With the increase of the C_nTAB monomers in the complex, the contribution of the negative contrast becomes more significant and therefore, more prominent in the $p(r)$ function.

A distinction in comparing the experimental SAXS data of α-LA bound by various concentrations of C_nTAB with the theoretical scattering of α-LA (PDB 1A4V) was performed by CRYSOL. As seen from Fig. 5A, the good fitting of experimental scattering profile of native α-LA with that of theoretical scattering of atomic structure is characterized by an χ^2 value of 1.52, suggesting that the compact structure of α-LA in solution. And the poor fitting was observed between SAXS data of α-LA added by low concentration of C_nTAB and atomic structure of α-LA, suggesting that the structure of α-LA was modified upon C_nTAB bound and a micelle-like conformation of the complex formed. Moreover, the structural parameters of the α-LA-C_nTAB complex, such as radius of gyration (R_g), D_{max}, and Porod volume increased upon bound by longer alkyl chain C_nTAB (Fig. 5B and Fig. S7). With the increasing chain length of C_nTAB (Fig. 5C), the dimensionless Kratky plot of α-LA exhibited a similar bell shape with an enhancement at a high-q region and the maximum intensity shifted slightly to the low-q region. For a completely unfolded protein or protein in a pre-MG state, the maximum intensity in the Kratky plot is hard to be observed, which is clearly indicative of an MG conformation of α-LA bound by longer chain C_nTAB [53].

Moreover, the reconstructed *ab initio* envelop of α-LA with a low concentration of C_nTAB has been performed by DAMMIN, reflecting the protein conformation in the initial binding stage. As shown in Fig. 5D,

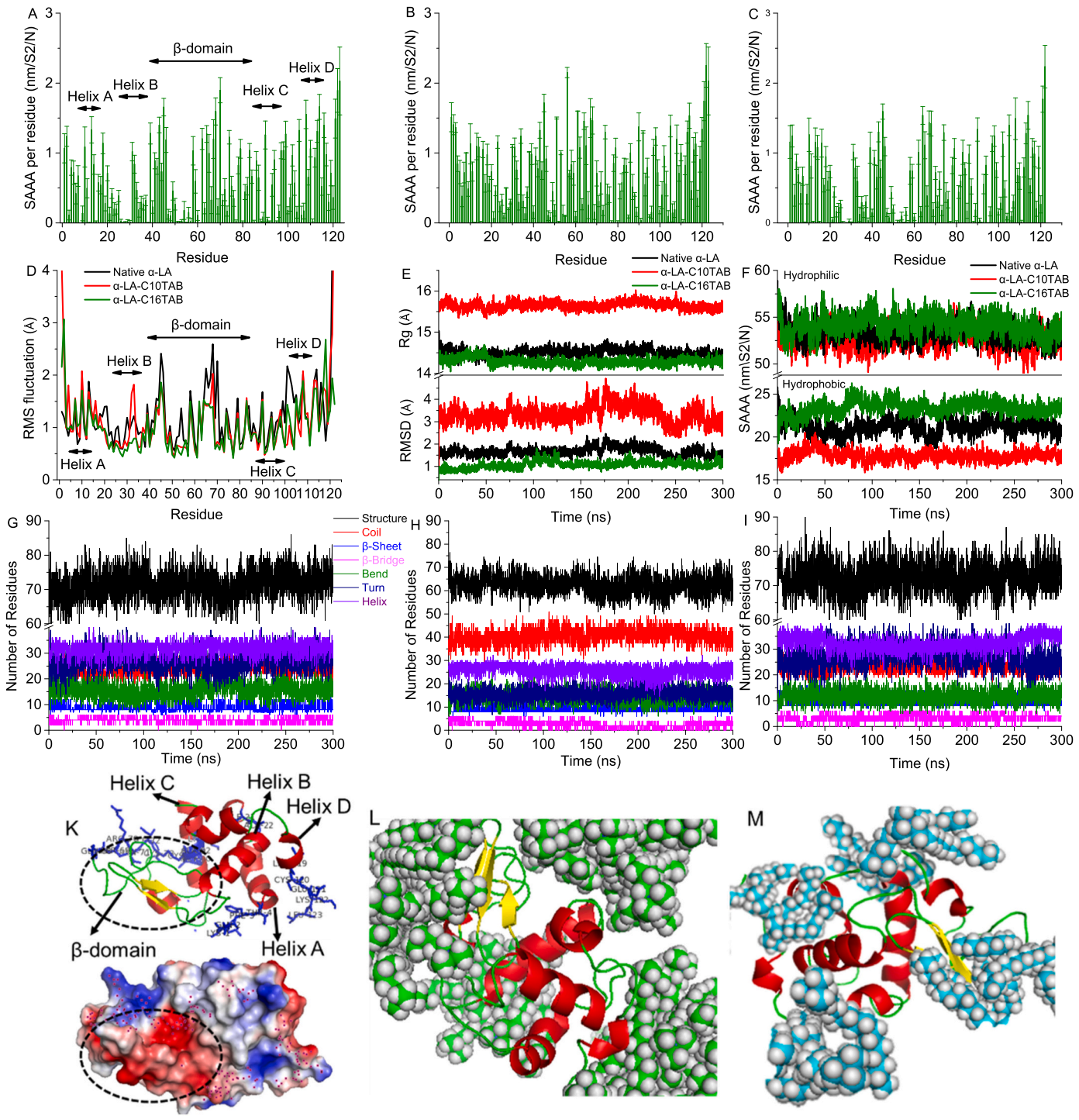

Fig. 6. The time-course of the binding of α-LA with C_nTAB during simulations. A-C: SASA of native α-LA, α-LA-C10TAB and α-LA-C16TAB complex, respectively. D: The RMSF analysis as function of α-LA residues. E: The value of RMSD and R_g for α-LA in the presence of C10TAB and C16TAB. F-I: Hydrophilic and hydrophobic SASA, and the secondary structure elements of α-LA bound by C10TAB and C16TAB. K: Schematic representation and electrostatic potential (red and blue: negative and positive charged) of α-LA and corresponding domain are highlighted. L-M: The last trajectory structural clustering of α-LA bound by C10TAB and C16TAB.

the excellent agreement between experimental SAXS data and DAMMIN modeling curve is indicated by χ^2 values close to 1.0. The *ab initio* bead model of the α-LA-C_nTAB complex exhibits an expanded shape in solution (Fig. 5E), demonstrating a modified tertiary structure of protein induced by C_nTAB and a conformation containing more water molecules. This is consistent with the description of the MG state as an ensemble of compact structure with persistent secondary structure but disrupted tertiary interactions and extensive solvent penetration of the hydrophobic core [54]. Interestingly, the increased envelope is found in the random coil and cleft region of α-LA, which is in line with the spectral results that C_nTAB induced an MG state α-LA upon binding with the random coil and cleft segment of protein. The longer chain C_nTAB providing more hydrophobic interactions prompted association with the unfolded segment(s) of protein and helped protein refold. It should be noted that the *ab initio* model represents the average of an ensembled conformation and the DAMMIN simulation of protein under large

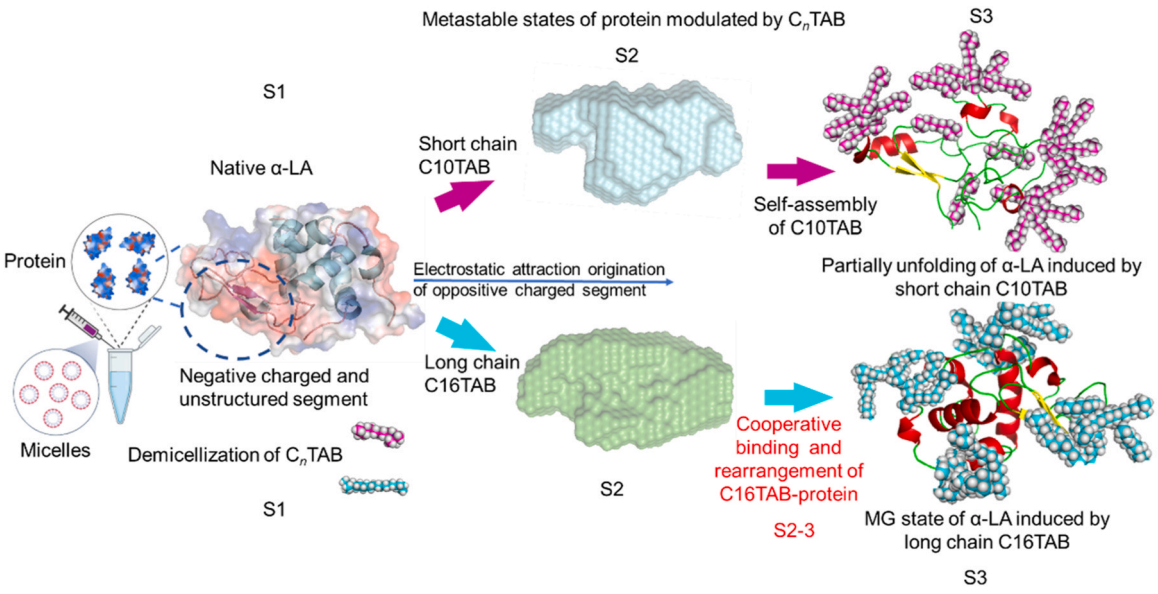

Fig. 7. Scheme of different state of α-LA modulated by C_nTAB. Some icons were from Biorender.

amounts of surfactant is not recommended since this modeling approach assumes a constant electron density for the simulated model. The SAXS results confirm that C_nTAB disrupted the tertiary structure of α-LA, and C16TAB induced an MG state of α-LA with the micelle-like structure even for surfactant concentrations below CMC.

3.4. Molecular dynamics (MD) simulations

The all-atom molecular dynamics (MD) simulations in 300 ns scale were performed to explain the molecular structure changes of α-LA bound by C_nTAB [55]. It can be observed from Fig. 6A-C that the solvent accessible surface area (SASA) of α-LA exhibited a higher value in the connecting loops and unstructured N-termini and C-termini, which was also found in the root-mean-square-fluctuation (RMSF) (Fig. 6D). With binding of C10TAB, a considerable increase of SASA value in the β-domain and the region between helix A and helix B was observed, suggesting a partially unfolded protein upon C10TAB bound. After the addition of C16TAB, the SASA value decreased in the random coil and unstructured termini, and the protein underwent the large conformational fluctuations in the loop between the helix B and the random coil region of the β-domain. The release of structured water emanates from the transfer of nonpolar surfaces into the protein's hydrophobic core accompanying a decrease in the heat capacity following complex formation and thus leading to an increased SASA [56]. These conformational fluctuations are presented by the residues 1–10, 35–50 and 60–70, which locates in the unstructured regions, loops connecting secondary structural elements and termini of α-LA [54]. This result suggests that the association of α-LA with C_nTAB consists of several hydration contributions which justify a significant role of hydrophobic interaction force underlying the binding process [36].

By adding C10TAB (Fig. 6E), α-LA presented an R_g of 16 Å with a root-mean-squared-deviation (RMSD) of 3 Å with a considerable decrease in helical structure and an increase in random coil (Fig. 6H). After adding C16TAB, the R_g and RMSD value was calculated as 14.4 Å and 1 Å, respectively. The stability of the major secondary structural elements of α-LA was similar to that of native protein, meaning an MG state of protein upon C16TAB bound (Fig. 6I). This is in line with the results of CD, fluorescence, and NMR spectra that an ensemble of the compact structure of α-LA with persistent secondary structure, but little tertiary structure upon bound by longer alkyl chain C_nTAB. Fig. 6F also shows that the hydrophobic interactions are the main forces to stabilize the α-LA-C_nTAB complex and dominate the structural change of the α-LA modulated by C_nTAB. This is also consistent with the ITC result that C_nTAB with longer chain shows more significant binding and thermodynamic parameters with α-LA. At neutral conditions, the β-domain of α-LA, a main unstructured segment, is negatively charged (Fig. 6K), making the electrostatic attraction crucial in the original orientation. Subsequently, the cooperative association of the longer chains C_nTAB molecules aligned along the prospective helix to stabilize exposed hydrophobic side chains of protein, which converted the loops or unstructured regions into α-helix. This result agrees with the SAXS modeling result that the increased DAMMIN envelop was found in the random coil and cleft area of α-LA. As a nonionic surfactant, polysorbate 20 also improved the α-helix and β-sheet content of casein and induced an MG state protein [6], even though little electrostatic interactions were involved. This indicates that hydrophobic interactions play a primary role in the modulation of the MG state protein. The last step trajectory during the simulation of α-LA-C10TAB and α-LA-C16TAB presented a micelle-like structure (Fig. 6L and M), where the positively charged C_nTAB group was energetically favorable to anchor the oppositive charged segment of protein, and the alkyl chain of C10TAB was not sufficient to bind with exposed hydrophobic paths of protein but was preferable to self-assemble, which led a partially unfolded protein. While C16TAB with a longer alkyl chain provided adequate hydrophobic interactions for associating with the unfolded regions to induce an MG state of the protein.

4. Conclusions

In this work, the interactions of α-LA with C_nTAB have been studied to explore the role of hydrophobic interactions in the MG state of globular protein modulated by surfactants. As indicated in Fig. 7 and Fig. S8, the binding of α-LA to C_nTAB undergoes four major steps: (S1) demicellization of C_nTAB micelles when diluted into α-LA solution. (S2): The orientation of ammonium bromide groups to the negatively charged and the unstructured segments of the protein. (S3): Further increasing C_nTAB monomers, the alkyl chain of C10TAB energetically preferable to self-assemble rather than associate with exposed unstructured regions of the protein, which leads to a partially unfolded protein. On the other hand, C16TAB, with a longer alkyl chain, provides adequate hydrophobic interactions and cooperatively binds to the unstructured regions of protein, forming a micelle-like structure and inducing an MG state. The α-domain of the protein comprising the highly structured parts and helices is found to be relatively stable, while the loops connecting

secondary structural elements, termini are disrupted upon binding with C_nTAB. (S4): The binding reaches saturation and free C_nTAB micelles form. This work not only provides molecular insights into the role of hydrophobic interactions in the intermediate states of globular protein induced by surfactants but also better understand the mechanism of preparing α-LA-based biomaterial modulated by hydrophobic interactions.

CRediT authorship contribution statement

Yang Sun: Conceptualization, Methodology, Software, Data curation, Methodology, Software, Funding acquisition, Investigation, Project administration, Writing - original draft, Writing - review & editing. **Pedro L. Oseliero Filho:** Data curation, Methodology, Software. **Yang Song, Zhichun Wang and Hang Ji:** Experiment validation. **Cristiano L. P. Oliveira:** Conceptualization, Methodology, Software, Funding acquisition, Supervision.

Conflict of interest

We wish to draw the attention of the Editor to the following facts which may be considered as potential conflicts of interest and to significant financial contributions to the manuscript with the title of "The role of hydrophobic interactions in the metastable states of globular protein modulated by surfactants".

We confirm that the manuscript has been read and approved by all named authors and that there are no other persons who satisfied the criteria for authorship but are not listed. We further confirm that the order of authors listed in the manuscript has been approved by all of us.

We confirm that we have given due consideration to the protection of intellectual property associated with this work and that there are no impediments to publication, including the timing of publication, with respect to intellectual property. In so doing we confirm that we have followed the regulations of our institutions concerning intellectual property.

We understand that the Corresponding Author is the sole contact for the Editorial process (including Editorial Manager and direct communications with the office). He is responsible for communicating with the other authors about progress, submissions of revisions and final approval of proofs. We confirm that we have provided a current, correct email address which is accessible by the Corresponding Author and which has been configured to accept email from sunyang@hbuas.edu.cn.

Data availability

Data will be made available on request.

Acknowledgement

We are grateful to Prof. Teresa Lamy, Dr. Evandro Duarte, Prof. Shirley Schreier, Dr. Jose Bozelli Jr. and Dr. Valquiria Souza for collection of spectra. We thank staffs at BL19U2 beamline of NFPS at SSRF for assistance with data collection. This work is supported by FAPESP (13/09604–6), Yunnan Basic Research Program (202201AT070031), Yunnan Xingdian Talent (XDYC-QNRC-2022–0739), CNPq, CAPES and INCT-FCx.

Appendix A. Supporting information

Supplementary data associated with this article can be found in the online version at doi:10.1016/j.colsurfb.2023.113490.

References

[1] K.K. Andersen, C.L. Oliveira, K.L. Larsen, F.M. Poulsen, T.H. Callisen, P. Westh, J. S. Pedersen, D. Otzen, The role of decorated SDS micelles in Sub-CMC protein denaturation and association, J. Mol. Biol. 391 (2009) 207–226.
[2] C. Højgaard, H.V. Sørensen, J.S. Pedersen, J.R. Winther, D.E. Otzen, Can a charged surfactant unfold an uncharged protein? Biophys. J. 115 (2018) 2081–2086.
[3] D.E. Otzen, Proteins in a brave new surfactant world, Curr. Opin. Colloid Interface Sci. 20 (2015) 161–169.
[4] D. Otzen, Protein–surfactant interactions: a tale of many states, Biochim. Et. Biophys. Acta (BBA) - Proteins Proteom. 1814 (2011) 562–591.
[5] Y. Sun, P.L. Oseliero, C.L.P. Oliveira, alpha-Lactalbumin and sodium dodecyl sulfate aggregates: denaturation, complex formation and time stability, Food Hydrocoll. 62 (2017) 10–20.
[6] X. Hu, X. Zhang, D. Chen, N. Li, Y. Hemar, B. Yu, S. Tang, Y. Sun, How much can we trust polysorbates as food protein stabilizers - the case of bovine casein, Food Hydrocoll. 96 (2019) 81–92.
[7] F. Cao, Y. Xia, D. Chen, N. Xu, Y. Hemar, N. Li, Y. Sun, Insights on the structure of caseinate particles based on surfactants-induced dissociation, Food Hydrocoll. 104 (2020), 105766.
[8] A.H. Poghosyan, N.P. Schafer, J. Lyngsø, A.A. Shahinyan, J.S. Pedersen, D.E. Otzen, Molecular dynamics study of ACBP denaturation in alkyl sulfates demonstrates possible pathways of unfolding through fused surfactant clusters, Protein Eng., Des. Sel. 32 (2019) 175–190.
[9] G.V. Jensen, J.N. Pedersen, D.E. Otzen, J.S. Pedersen, Multi-step unfolding and rearrangement of α-lactalbumin by SDS revealed by stopped-flow SAXS, Front. Mol. Biosci. 7 (2020).
[10] J.N. Pedersen, J. Lyngsø, T. Zinn, D.E. Otzen, J.S. Pedersen, A complete picture of protein unfolding and refolding in surfactants, Chem. Sci. 11 (2020) 699–712.
[11] S. Sengupta, R. Gera, C. Egan, U.N. Morzan, J. Versluis, A. Hassanali, H.J. Bakker, Observation of strong synergy in the interfacial water response of binary ionic and nonionic surfactant mixtures, J. Phys. Chem. Lett. 13 (2022) 11391–11397.
[12] D. Saha, D. Ray, J. Kohlbrecher, V.K. Aswal, Unfolding and refolding of protein by a combination of ionic and nonionic surfactants, Acs Omega 3 (2018) 8260–8270.
[13] K.K. Andersen, D.E. Otzen, How chain length and charge affect surfactant denaturation of acyl coenzyme a binding protein (ACBP), J. Phys. Chem. B 113 (2009) 13942–13952.
[14] J. Goers, S.E. Permyakov, E.A. Permyakov, V.N. Uversky, A.L. Fink, Conformational prerequisites for alpha-lactalbumin fibrillation, Biochemistry 41 (2002) 12546–12551.
[15] C. Redfield, B.A. Schulman, M.A. Milhollen, P.S. Kim, C.M. Dobson, alpha-lactalbumin forms a compact molten globule in the absence of disulfide bonds, Nat. Struct. Biol. 6 (1999) 948–952.
[16] M. Mizuguchi, K. Masaki, M. Demura, K. Nitta, Local and long-range interactions in the molten globule state: a study of chimeric proteins of bovine and human alpha-lactalbumin, J. Mol. Biol. 298 (2000) 985–995.
[17] G. Böhm, R. Muhr, R. Jaenicke, Quantitative analysis of protein far UV circular dichroism spectra by neural networks, Protein Eng. 5 (1992) 191–195.
[18] E.D. Chrysina, K. Brew, K.R. Acharya, Crystal structures of apo- and holo-bovine α-lactalbumin at 2.2 Å; resolution reveal an effect of calcium on inter-lobe interactions, J. Biol. Chem. 275 (2000) 37021–37029.
[19] K. Takeda, K. Ogawa, M. Ohara, S. Hamada, Y. Moriyama, Conformational changes of α-lactalbumin induced by the stepwise reduction of its disulfide bridges: the effect of the disulfide bridges on the structural stability of the protein in sodium dodecyl sulfate solution, J. Protein Chem. 14 (1995) 679–684.
[20] Y. Moriyama, N. Kondo, K. Takeda, Secondary structural changes of homologous proteins, lysozyme and α-lactalbumin, in thermal denaturation up to 130 °c and sodium dodecyl sulfate (SDS) effects on these changes: comparison of thermal stabilities of SDS-induced helical structures in these proteins, Langmuir 28 (2012) 16268–16273.
[21] S. Hamada, K. Takeda, Conformational changes of α-lactalbumin and its fragment, Phe31-Ile59, induced by sodium dodecyl sulfate, J. Protein Chem. 12 (1993) 477–482.
[22] N. Li, X.H. Li, Y.Z. Wang, G.F. Liu, P. Zhou, H.J. Wu, C.X. Hong, F.G. Bian, R. G. Zhang, The new NCPSS BL19U2 beamline at the SSRF for small-angle X-ray scattering from biological macromolecules in solution, J. Appl. Crystallogr. 49 (2016) 1428–1432.
[23] J.B. Hopkins, R.E. Gillilan, S. Skou, BioXTAS RAW: improvements to a free open-source program for small-angle X-ray scattering data reduction and analysis, J. Appl. Crystallogr. 50 (2017) 1545–1553.
[24] D. Franke, M.V. Petoukhov, P.V. Konarev, A. Panjkovich, A. Tuukkanen, H.D. T. Mertens, A.G. Kikhney, N.R. Hajizadeh, J.M. Franklin, C.M. Jeffries, D. I. Svergun, ATSAS 2.8: a comprehensive data analysis suite for small-angle scattering from macromolecular solutions, J. Appl. Crystallogr. 50 (2017) 1212–1225.
[25] D.I. Svergun, C. Barberato, M.H.J. Koch, CRYSOL– a program to evaluate X-ray solution scattering of biological macromolecules from atomic coordinates, J. Appl. Crystallogr. 28 (1995) 768–773.
[26] D.I. Svergun, Restoring low resolution structure of biological macromolecules from solution scattering using simulated annealing, Biophys. J. 76 (1999) 2879–2886.
[27] V.V. Volkov, D.I. Svergun, Uniqueness of ab initio shape determination in small-angle scattering, J. Appl. Crystallogr. 36 (2003) 860–864.
[28] M.B. Kozin, D.I. Svergun, Automated matching of high- and low-resolution structural models, J. Appl. Crystallogr. 34 (2001) 33–41.

[29] B. Hess, N.F.A. van der Vegt, Hydration thermodynamic properties of amino acid analogues: a systematic comparison of biomolecular force fields and water models, J. Phys. Chem. B 110 (2006) 17616–17626.
[30] M.M. Cassiano, J.A.G. Areas, Study of bovine beta-casein at water/lipid interface by molecular modeling, J. Mol. Struct. Theochem. 539 (2001) 279–288.
[31] H.J.C. Berendsen, J.P.M. Postma, W.Fv Gunsteren, A. DiNola, J.R. Haak, Molecular dynamics with coupling to an external bath, J. Chem. Phys. 81 (1984) 3684–3690.
[32] W. Kabsch, C. Sander, Dictionary of protein secondary structure - pattern-recognition of hydrogen-bonded and geometrical features, Biopolymers 22 (1983) 2577–2637.
[33] A.K. Malde, L. Zuo, M. Breeze, M. Stroet, D. Poger, P.C. Nair, C. Oostenbrink, A. E. Mark, An automated force field topology builder (ATB) and repository: version 1.0, J. Chem. Theory Comput. 7 (2011) 4026–4037.
[34] M. Sammalkorpi, M. Karttunen, M. Haataja, Structural properties of ionic detergent aggregates: a large-scale molecular dynamics study of sodium dodecyl sulfate, J. Phys. Chem. B 111 (2007) 11722–11733.
[35] M.D. Lad, V.M. Ledger, B. Briggs, R.J. Green, R.A. Frazier, Analysis of the SDS-lysozyme binding isotherm, Langmuir 19 (2003) 5098–5103.
[36] B.K. Paul, N. Ghosh, S. Mukherjee, Binding of norharmane with RNA reveals two thermodynamically different binding modes with opposing heat capacity changes, J. Colloid Interface Sci. 538 (2019) 587–596.
[37] L. Feng, J.D. Andrade, Protein adsorption on low-temperature isotropic carbon.1. Protein conformational change probed by differential scanning calorimetry, J. Biomed. Mater. Res. 28 (1994) 735–743.
[38] N.R. Syme, C. Dennis, S.E.V. Phillips, S.W. Homans, Origin of heat capacity changes in a “nonclassical” hydrophobic interaction, ChemBioChem 8 (2007) 1509–1511.
[39] S.W. Rick, Heat capacity change of the hydrophobic interaction, J. Phys. Chem. B 107 (2003) 9853–9857.
[40] B.K. Paul, N. Ghosh, S. Mukherjee, Interaction of an anti-cancer photosensitizer with a genomic DNA: from base pair specificity and thermodynamic landscape to tuning the rate of detergent-sequestered dissociation, J. Colloid Interface Sci. 470 (2016) 211–220.
[41] K. Koga, L.J. Berliner, Structural elucidation of a hydrophobic box in bovine alpha-lactalbumin by NMR - nuclear overhauser effects, Biochemistry 24 (1985) 7257–7262.
[42] S. Chakraborty, V. Ittah, P. Bai, L. Luo, E. Haas, Z.Y. Peng, Structure and dynamics of the alpha-lactalbumin molten globule: Fluorescence studies using proteins containing a single tryptophan residue, Biochemistry 40 (2001) 7228–7238.
[43] J.X. Song, P. Bai, L. Luo, Z.Y. Peng, Contribution of individual residues to formation of the native-like tertiary topology in the alpha-lactalbumin molten globule, J. Mol. Biol. 280 (1998) 167–174.
[44] L.C. Wu, P.S. Kim, A specific hydrophobic core in the alpha-lactalbumin molten globule, J. Mol. Biol. 280 (1998) 175–182.
[45] A. Chaudhuri, A. Chattopadhyay, Lipid binding specificity of bovine α-lactalbumin: a multidimensional approach, Biochim. Et. Biophys. Acta (BBA) - Biomembr. 1838 (2014) 2078–2086.
[46] H.A. Benesi, J.H. Hildebrand, A spectrophotometric investigation of the interaction of iodine with aromatic hydrocarbons, J. Am. Chem. Soc. 71 (1949) 2703–2707.
[47] J. Balbach, V. Forge, N.A.J. van Nuland, S.L. Winder, P.J. Hore, C.M. Dobson, Following protein folding in real time using NMR spectroscopy, Nat. Struct. Biol. 2 (1995) 865–870.
[48] Ø. Halskau, J. Underhaug, N.Å. Frøystein, A. Martínez, Conformational flexibility of α-lactalbumin related to its membrane binding capacity, J. Mol. Biol. 349 (2005) 1072–1086.
[49] S. Ramboarina, C. Redfield, Structural characterisation of the human α-lactalbumin molten globule at high temperature, J. Mol. Biol. 330 (2003) 1177–1188.
[50] Ø. Halskau, N.Å. Frøystein, A. Muga, A. Martínez, The membrane-bound conformation of α-lactalbumin studied by NMR-monitored 1H exchange, J. Mol. Biol. 321 (2002) 99–110.
[51] R. Wijesinha-Bettoni, C.M. Dobson, C. Redfield, Comparison of the denaturant-induced unfolding of the bovine and human α-lactalbumin molten globules, J. Mol. Biol. 312 (2001) 261–273.
[52] Y. Sun, X. Li, R. Chen, F. Liu, S. Wei, Recent advances in structural characterization of biomacromolecules in foods via small-angle X-ray scattering 9 (2022).
[53] Y. Wang, J.B. Jiang, Y.C. Gao, Y. Sun, J.F. Dai, Y. Wu, D. Qu, G. Ma, X.Y. Fang, Staphylococcus epidermidis small basic protein (Sbp) forms amyloid fibrils, consistent with its function as a scaffolding protein in biofilms, J. Biol. Chem. 293 (2018) 14296–14311.
[54] M. Tarek, D.A. Neumann, D.J. Tobias, Characterization of sub-nanosecond dynamics of the molten globule state of α-lactalbumin using quasielastic neutron scattering and molecular dynamics simulations, Chem. Phys. 292 (2003) 435–443.
[55] H. Zou, Z. Xu, L. Zhao, Y. Wang, X. Liao, Effects of high pressure processing on the interaction of α-lactalbumin and pelargonidin-3-glucoside, Food Chem. 285 (2019) 22–30.
[56] D. Ondo, M. Costas, Complexation thermodynamics of α-cyclodextrin with ionic surfactants in water, J. Colloid Interface Sci. 505 (2017) 445–453.